AN EXPERIMENTAL SETUP FOR THE STUDY OF THE PARTICLES STORED IN AN ELECTRODYNAMIC LINEAR TRAP

GINA VISAN[1], OVIDIU S. STOICAN[1]

[1] National Institute for Laser, Plasma and Radiation Physics, Atomistilor Str.409, RO-077125 Magurele-Bucharest, Romania, E-mail: stoican@infim.ro

Received March 26, 2012

A system to study the micrometer sized particles dynamic stored in a linear electrodynamic trap, at normal temperature and pressure, is reported. The variations with time of the light intensity scattered by the stored particles are recorded and analyzed in the frequency domain. Experimental and numerical results are compared.

Key words: Charged particle trapping, electrodynamic trap, photodetector, lock-in amplifier.

1. INTRODUCTION

Electrode systems generating an alternating quadrupole electric field allow the confinement of the micrometer sized particles (microparticles) in a small region of space. Usually, these kinds of devices are called electrodynamic traps. Its design is based on the principle of the radiofrequency quadrupole trap used to store ions in ultrahigh vacuum first proposed by W. Paul in 1953. At present, the ion trapping techniques are used for a wide range of applications, from the mass spectrometry [1–3] and atomic frequency standards [4, 5] to the quantum computation and preparation of the ultracold quantum gases by using laser cooling [6–9].

An electrodynamic trap allows maintaining different species of solid and liquid macroscopic particles, at atmospheric pressure, without physical contact with the wall of a container. This important feature makes possible utilization them as a device aimed to hold the sample for the various laboratory instruments used to study properties of dust particles [10], aerosols [11–14], liquid droplets [15, 16] or microorganisms [17]. The purpose of this paper is to describe an experimental setup able to determine the harmonic components frequency of the microparticles motion (motional spectrum), stored in a linear electrodynamic trap at normal temperature and pressure. Comparing the harmonic components frequency obtained as a result of numerical simulations with those experimentally measured one could estimate the physical characteristics of the stored particles and operating point of the trap. The system is also intended to study the effect of different external

forces on the stored microparticles. The measurement chain consists of a modulated laser source, a photodetector, a phase sensitive demodulator (lock-in amplifier) and a spectrum analyzer. This approach represents an improvement of the setup described in [18, 19] where the laser beam was not modulated and the photodetector output voltage has been applied directly to the input of a spectrum analyzer.

2. ELECTRODYNAMIC TRAP LAYOUT

A linear electrodynamic trap consists of four identically brass rods: E1, E2, E3, E4, equidistantly spaced and two "endcap" electrodes: E5, E6. The electrode E1 is connected to the laboratory ground. A high ac sinusoidal voltage $V_{ac} = V_0 \cos 2\pi f_0 t$ is applied to the electrodes E2 and E3. The gravity force is balanced by a dc voltage U_x applied between the electrodes E1 and E4. Another dc voltage U_z is applied to the endcap electrodes E5, E6 in order to assure the axial stability of the stored particles. Spatial arrangement and electrical circuit of the electrodes for a linear electrodynamic trap is shown schematically in Figure 1.

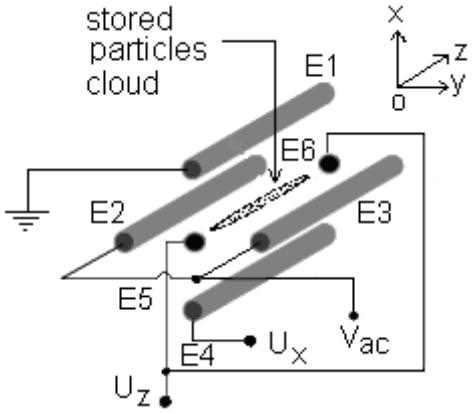

Fig. 1 – Spatial arrangement and electrical circuit of the electrodes for a linear electrodynamic trap.

To block air streams the whole trap is enclosed in a transparent plastic box. The charged microparticles are stored on the longitudinal axis of the electrodynamic trap, at normal pressure and temperature, for hours, in a quasi interaction free environment. In Figure 2 a representative image of a stored microparticles cloud is shown. Polarity of the voltage U_x can be reversed. By varying the magnitude of the voltage U_x and/or changing its polarity the stored particles cloud can be displaced vertically. The necessary dc voltages U_x and U_z, amplitude V_0 and frequency f_0 of the ac voltage depend on the physical dimensions

of the trap and particles size. In the case of a trap with the distance between rod electrodes of the order of a centimeter and distance between endcap electrodes of a few centimeters, the dc voltages U_x and U_z can be varied in the range 0 –1000V, while ac voltage V_{ac} is on the order of 1– 4kV$_{rms}$ at a frequency from 40 to 100 Hz. More details on the mechanical layout and electrical supply of the linear electrodynamic traps can be found in [19, 20].

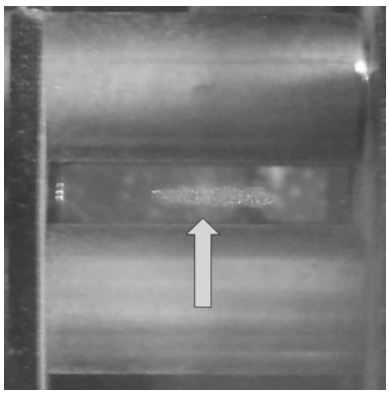

Fig. 2 – Microparticles cloud (pointed by the arrow) stored along the longitudinal axis of the linear trap [19].

3. MEASUREMENT CHAIN

The design of the measurement chain is similar to the method described in [10] implemented to a linear electrodynamic trap. Advantages of a linear trap compared to a classical quadrupole trap are: a lot of particles are confined in a narrow region along the longitudinal symmetry axis; capability to store a large number of particles; good optical access; simple mechanical layout. The block diagram of the measurement chain is shown in Figure 3. The output beam (incident radiation) of a low power laser diode is directed along the axis of the linear trap. For this purpose a hole was drilled into one of the endcap electrode (E6) allowing the passing of the laser beam. The maximum illumination of the stored microparticles cloud is achieved by adjusting properly the voltage U_x. The incident laser beam is modulated on/off at a frequency f_s much higher than that of ac voltage ($f_s >> f_0$). A photodetector PD is directed normal to the linear trap longitudinal axis. A certain amount of the radiation scattered by the stored particles is received by the photodetector and converted into an electrical signal. Therefore, the photodetector provides an electric signal only if there are stored particles in the trap region crossed by the laser beam. The resulting electrical voltage U_{ph} at the output of the photodetector represents a series of pulses of variable amplitude at fixed frequency f_s. This electrical signal is applied to the input of a lock-in amplifier. The voltage

U_s, driving the functional block which modulates on/off the laser beam, is used as the lock-in reference signal. In this way only photodetector signal components coherently (same frequency and phase) with laser beam pulses are amplified and demodulated. The parasitic signals, especially due to the ac voltage applied to the trap electrodes or mains hum, are rejected. The motion of the stored particles modulates the intensity of the scattered optical radiation collected by the photodetector. Consequently, after demodulation, photodetector output voltage contains the same harmonic components. A spectrum analyzer is used to perform Fourier transform of the time varying signal provided by the lock-in amplifier allowing the frequency domain analysis of the radiation scattered by the stored particles.

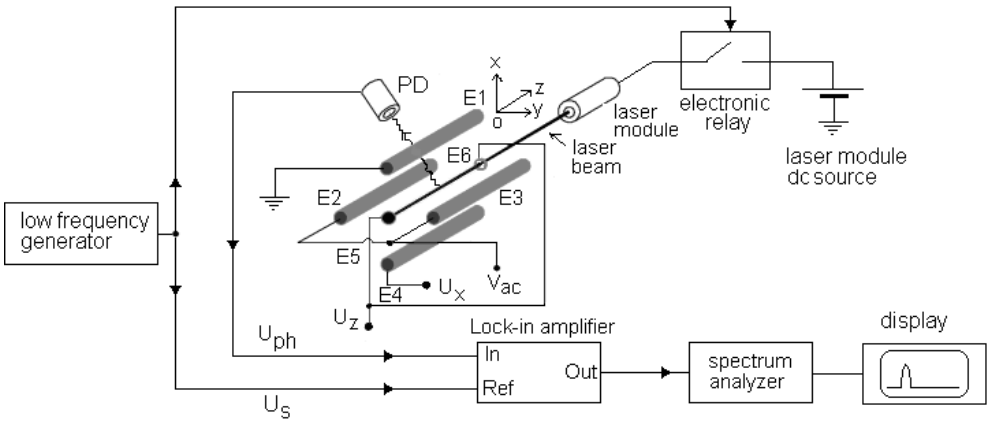

Fig. 3 – Block diagram of the measurement chain.

Practical realization of the measurement chain includes a Burr-Brown OPT301 integrated circuit as the photodetector. According to its datasheet, OPT301 is an optoelectronic device containing a photodiode and a transimpedance amplifier integrated on a single dielectrically isolated chip [21]. Following the design recommended by the manufacturer, an appropriate electronic circuit has been added in order to reject unwanted steady state background light and to improve the signal to noise ratio by amplifying the photodetector output signal (Figure 4). As a result the assembly consisting of photodetector and electronic circuit acts as a high pass filter characterized by cutoff frequency f_c given by formula [21]:

$$f_c = \frac{1M\Omega}{R_3(2\pi R_2 C_2)} \tag{1}$$

Taking into account values assigned to the electronic circuit components, the cutoff frequency $f_c \approx 16$Hz. To prevent electrical perturbations due to the existing ac high voltage applied to the electrodes trap, the photodetector itself and associated electronic circuit are encapsulated in a grounded cylindrical shielding box. A low power laser module (650 nm, 3 mW) represents the source of the laser beam. By means of an electronic relay which switches the laser module supply current, the laser beam is modulated on/off. During measurements the switching frequency f_s has been kept at 2kHz. The electrical signal provided by the photodetector circuit is amplified and demodulated by a lock-in amplifier Stanford Research SR830. A common data acquisition board connected to a computer is used to record and process the output signal. By using a FFT software the relative amplitude of the low frequency harmonic components of the optical radiation intensity scattered by the stored particles are displayed on the computer screen.

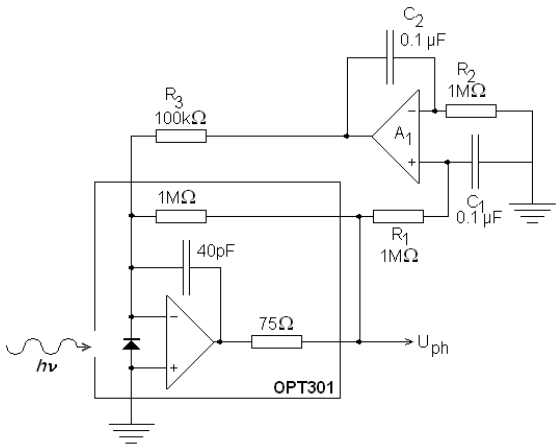

Fig. 4 – Electronic circuit of the photodetector [21].

4. NUMERICAL CALCULATION OF THE STORED PARTICLE MOTIONAL SPECTRUM FOR A PARTICULAR TRAP OPERATING POINT

Because the motion of a charged particle in a quadrupole electric field is very well known (*e.g.* [2, 22, 23]), only the basic equations used for our numerical analysis will be summarized here. For an ideal electrodynamic trap, in the region of the longitudinal axis ($x,\ y << R$), the electric potential may be expressed approximately as [22]:

$$\Phi(x,y,t) = \frac{x^2 - y^2}{2R^2}(U_0 + V_0 \cos \Omega t) \tag{2}$$

where R is the radial distance from the longitudinal axis to the rod electrodes and $\Omega=2\pi f_0$. Therefore, equations of motion for a charged particle of mass M and charge Q are:

$$\frac{\mathrm{d}^2x}{\mathrm{d}\xi^2}+\delta\frac{\mathrm{d}x}{\mathrm{d}\xi}+(a_x+2q_x\cos 2\xi)x=0 \tag{3}$$

$$\frac{\mathrm{d}^2y}{\mathrm{d}\xi^2}+\delta\frac{\mathrm{d}y}{\mathrm{d}\xi}+(a_y+2q_y\cos 2\xi)y=0 \tag{4}$$

where frictional terms $-\delta\frac{\mathrm{d}x}{\mathrm{d}\xi}$, $-\delta\frac{\mathrm{d}y}{\mathrm{d}\xi}$ describe the drag force exerted on the particle moving in air. The dimensionless parameters $a_{x,y}$, $q_{x,y}$, ξ and δ are given by: $a_x=-a_y=a=\frac{4QU_0}{M\Omega^2R^2}$, $q_x=-q_y=q=\frac{2QV_0}{M\Omega^2R^2}$, $\xi=\Omega t/2$, $\delta=\frac{6\pi\eta d}{M\Omega}$, where d is the diameter of the charged particle, while η = 1.8 x 10^{-5}kgm^{-1}s^{-1} is air dynamic viscosity at normal temperature and pressure. If the frictional terms are neglected, each of differential equations (3) or (4) takes the form of a Mathieu equation [24]. Its general solution has the form:

$$u(\xi)=A_1\mathrm{e}^{\mu\xi}\sum_{n=-\infty}^{n=\infty}C_{2n}\mathrm{e}^{2in\xi}+A_2\mathrm{e}^{-\mu\xi}\sum_{n=-\infty}^{n=\infty}C_{2n}\mathrm{e}^{-2in\xi} \tag{5}$$

where $u(\xi)$ may be $x(\xi)$ or $y(\xi)$, A_1 and A_2 are constants which depend on the initial conditions, while coefficients C_{2n} and μ depend only on the parameters a and q. In the general case $\mu_{x,y}=\alpha_{x,y}+i\beta_{x,y}$ where $\alpha_{x,y}$ and $\beta_{x,y}$ are real functions depending on a and q [22, 24, 25].

It can be proved that solutions of a Mathieu equation describe a spatial bounded trajectory (stable solutions) only for certain areas of the (a,q) plane called stability regions, corresponding to $\alpha_{x,y}=0$ and $\beta_{x,y}\neq n$ where n is an integer. Outside of the stability regions, a particle will be ejected out of the trap, its motion amplitude increasing exponentially. The couples (a,q) for which $\beta_{x,y}(a,q)=n$, define the curves bounding the stability regions. The first stability region (bounded by the curves $\beta_{x,y}(a,q)=0$ and $\beta_{x,y}(a,q)=1$) corresponds to the lowest voltages applied to the trap electrodes. For $a=0$ and $q<<1$, $\beta\approx q/\sqrt{2}$, while for $a=0$ and $\beta\simeq 1$, $q(\beta)\approx 0.908047-1.39869(1-\beta)^2$ [2]. Therefore, in the case of the first stability region and a = 0, the stable solutions are obtained if $0<q<0.908\ldots$.

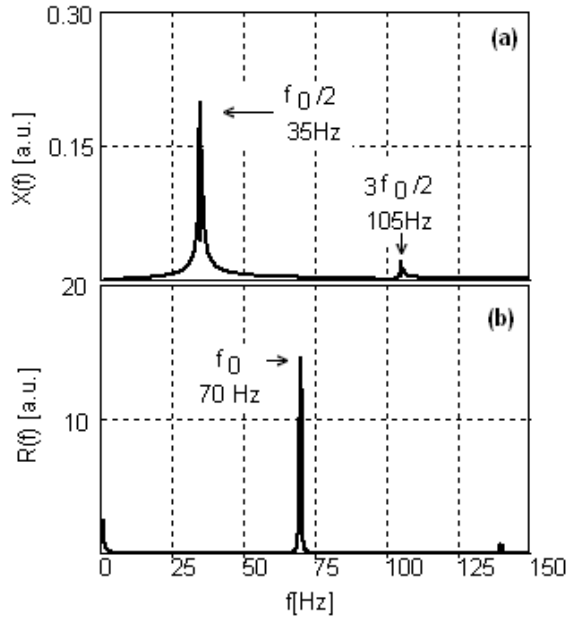

Fig. 5 – Fourier transform *X(f)* (a) and *R(f)* (b) of the rectangular *x(t)* and radial *r(t)* coordinates, respectively, for $q_x = 0.908$, $a_x = 0$, $f_0 = \Omega/2\pi = 70$Hz, $\delta = 0.01$. Numerical result.

Taking into account the frictional term, the first stability region is enlarged so that, depending on the value of δ, a particle can remain inside the trap even for $q \approx 0.908$. Near the upper bound of the first stability region the motion amplitude of the stored particle reaches a maximum but still remains lower than a finite value. This operating point of the trap is known as "spring point" [26]. Such experimental conditions can be achieved simply and are easily recognized. Fourier transforms *X(f)* and *R(f)*, of the rectangular *x(t)* and radial coordinates $r(t) = \sqrt{x^2(t) + y^2(t)}$, respectively, in the range from 0 to 150Hz, obtained by solving numerically differential equations (3) and (4) for an operating point of the trap close to the upper bound of the first stability region is shown in Figure 5. Fourier transforms of *y(t)* is similar to that of *x(t).* The numerical results show that, considering air friction, close to the upper bound of the first stability region, the motional spectrum contains only a few significant components, namely at f_0 for *r(t)* and at $f_0/2$ and $3f_0/2$ for *x(t),* respectively.

5. EXPERIMENTAL MEASUREMENT

Results derived by solving numerically the equations which describes the motion of a charged particle within an electrodynamic trap have been compared to those obtained by using the measurement setup above described. Experimental

observations were conducted using Al_2O_3 powder, 60-200 μm in diameter, stored at normal pressure and temperature. The working voltages (U_x, U_z and V_0) were chosen so that the magnitude of the harmonic component of U_{ph} corresponding to f_0 to reach a maximum. The spectrum of the signal at the output of the lock-in amplifier recorded in these experimental conditions is shown in Figure 6.

6. CONCLUSIONS

By comparing the recorded spectrum shown in Figure 6 with theoretical plots shown in Figure 5 it can be concluded that under assumed conditions, the spectrum of the laser radiation intensity scattered by the stored microparticles appears to be a superposition of the *r(t)* and *x(t)* (or *y(t)*) harmonic components, respectively. Taking into account the particular trap operating point, corresponding to the upper bound of the first stability region, $q_x \approx 0.908$ and specific charge can be estimated to be $Q/M \approx 0.6 \times 10^{-3}$C/kg. Distribution of the frequency peaks are identical both in experimental record and numerical simulation, but their relative heights are different. There are several causes for that. First of all we used a simplified theoretical approach, namely a single charged particle which is stored inside an ideal linear electrodynamic trap. In fact there is a cloud of charged particles characterized by a spatial electric charge while the actual trap is far from ideal one.

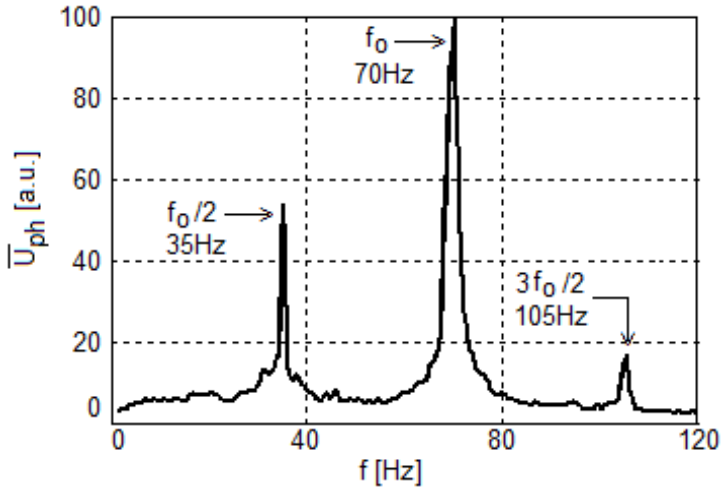

Fig. 6 – Spectrum of the lock-in amplifier output voltage near the upper bound of the first stability region. Experimental conditions: $f_0 = 70$Hz, $V_0 = 3.4$kV, $U_x = 330$V, $U_z = 920$V. Experimental result.

Thus, electric field distribution along the trap longitudinal axis may be different from that one described by (2). On the other side the electric field generated by the voltages U_x and U_z shifts the stored microparticles cloud position relative to the

trap longitudinal axis. Therefore, viewing angle of the photodetector is modified and amplitude of some harmonic components appears to be diminished. In spite of these problems which require some experimental precautions and a better theoretical model one could conclude that there is good qualitative agreement between experimental and numerical results.

Acknowledgments. The authors would like to thank Prof. Dr. Ioan Baltog for his permanent support and helpful comments. This work is done in the framework of the project PN 09390301.

REFERENCES

1. R. E. March, International Journal of Mass Spectrometry, **200**, 285–312 (2000).
2. D. J. Douglas, A. J. Frank, D. Mao, Mass Spectrometry Reviews, **24**, 1–29 (2005).
3. K. Blaum, Physics Reports **425**, 1–78 (2006).
4. J. D. Prestage, R. L. Tjoelker, and L. Maleki, Topics Appl. Phys. **79**, 195–211 (2001).
5. W. H. Oskay, S. A. Diddams, E. A. Donley, T. M. Fortier, T. P. Heavner, L. Hollberg, W. M. Itano, S. R. Jefferts, M. J. Delaney, K. Kim, F. Levi, T. E. Parker, J. C. Bergquist, Phys. Rev. Lett., **97**, 020801 (2006).
6. D. J. Wineland, W. M. Itano, Phys. Rev. A, **20**, 1521–1540 (1979).
7. J. I. Cirac, P. Zoller, Phys. Rev. Lett., **74**, 4091–4094 (1995).
8. C. Zipkes, L. Ratschbacher, C. Sias, M. Köhl, New Journal of Physics, **13**, 053020 (2011).
9. D. J. Wineland, C. Monroe, W. M. Itano, D. Leibfried, B. E. King, D. M. Meekhof, J. Res. Natl. Inst. Stand. Technol. **103**, 259–328 (1998).
10. S. Schlemmer, J. Illemann, S. Wellert, D. Gerlich, J. Appl. Phys. **90**, 5410–5418 (2001).
11. K. L. Carleton, D. M. Sonnenfroh, W. T. Rawlins, B. E. Wyslouzil, S. Arnold, Journal of Geophysical Research **102**, 6025–6033 (1997).
12. E. J. Davis, Aerosol Science and Technology, **26**, 212–254 (1997).
13. A. Kürten, J. Curtius, F. Helleis, E. R. Lovejoy, S. Borrmann, International Journal of Mass Spectrometry **265**, 30–39 (2007).
14. A. A. Zardini, S. Sjogren, C. Marcolli, U. K. Krieger, M. Gysel, E. Weingartner, U. Baltensperger, T. Peter, Atmos. Chem. Phys. **4**, 1997–2000 (2008).
15. R. A. Shaw, D. Lamb, A. M. Moyle, Journal of Atmospheric and Oceanic Technology **17**, 940–948 (2000).
16. B. Krämer, O. Hübner, H. Vortisch, L. Wöste, T. Leisnera, M. Schwell, E. Rühl, H. Baumgärtel, J. Chem. Phys. **111**, 6521–6527 (1999).
17. W. P. Peng, Y. C. Yang , M. W. Kang, Y. T. Lee, H. C. Chang, J. Am. Chem. Soc. **126**, 11766–11767 (2004).
18. O. S. Stoican, L. C. Dinca, G. Visan, S. Radan, Journal of Optoelectronics and Advanced Materials **10**, 1988–1990 (2008).
19. O. S. Stoican, Studies on the Interaction Between an Acoustic Wave and Levitated Microparticles, pp. 241–256 in *Wave in Fluids and Solids*, Prof. Ruben Pico Vila (Ed.), ISBN: 978-953-307-285-2, InTech, 2011.
20. V. N. Gheorghe, L. Giurgiu, O. Stoican, D. Cacicovschi, R. Molnar, B. Mihalcea, Acta Physica Polonica A **93**, 625–629 (1998).
21. *** Burr Brown Corporation, *OPT301 Datasheet*, 1994.

22. F. G. Major, V. N. Gheorghe, G. Werth, *Charged Particle Traps, Physics and Techniques of Charged Particle Confinement*, ISBN: 3-540-22043-7, Springer, Berlin Heidelberg New York, 2005.
23. R. E. March, Journal of Mass Spectrometry **32**, 351–369 (1997).
24. N. W. McLachlan, *Theory and Application of Mathieu Functions,* Clarendon Press, Oxford, 1947.
25. A. I. Nicolin, R. Carretero-González, P. G. Kevrekidis, Phys. Rev. A, **76**, 063609 (2007).
26. E. J. Davis, M. F. Buehler, L. T. Ward, Review of Scientific Instrument **61**, 1281–1288 (1990).